Journal of the Korean Ceramic Society
Vol. 44, No. 6, pp. 291~296, 2007.

Fabrication of Porous Al_2O_3-(m-ZrO_2) Composites and Al_2O_3-(m-ZrO_2)/PMMA Hybrid Composites by Infiltration Process

Byong-Taek Lee,† Do Van Quang, and Ho-Yeon Song*

Department of Biomedical Engineering and Materials, School of Medicine, Soonchunhyang University, Chungnam 330-090, Korea
**Department of Microbiology, School of Medicine, Soonchunhyang University, Chungnam 330-090, Korea*
(Received April 21, 2007; Accepted June 11, 2007)

ABSTRACT

Porous Al_2O_3-(m-ZrO_2) composites were fabricated by pressureless sintering, using different volume percentages (40%-60%) of poly methyl methacrylate (PMMA) powders as a pore-forming agent. The pore-forming agent was successfully removed, and the pore size and shape were well-controlled during the burn-out and sintering processes. The average pore size in the porous Al_2O_3-(m-ZrO_2) bodies was about 200 μm in diameter. The values of relative density, bending strength, hardness, and elastic modulus decreased as the PMMA content increased; i.e., in the porous body (sintered at 1500°C) using 55 vol % PMMA, their values were about 50.8%, 29.8 MPa, 266.4 Hv, and 6.4 GPa, respectively. To make the Al_2O_3-(m-ZrO_2)/polymer hybrid composites, a bioactive polymer, such as PMMA, was infiltrated into the porous Al_2O_3-(m-ZrO_2) composites. After infiltration, most of the pores in the porous Al_2O_3-(m-ZrO_2) composites, which were made using 60 vol % PMMA additions, were infiltrated with PMMA, and their values of relative density, bending strength, hardness, and elastic modulus remarkably increased.

***Key words*: Porous Al_2O_3-(m-ZrO_2) composites, Infiltration, Ceramic-polymer composites**

1. Introduction

Al_2O_3 and ZrO_2 ceramics have received a lot of attention due to their good biocompatibility and corrosion resistance, excellent chemical stability, and outstanding mechanical properties.[1-3] Due to an increase in the life-span of human beings and the industrial accidents, it is expected that the need for various types of artificial devices, especially ceramic implants, will increase. Consequently, the development of porous Al_2O_3 and ZrO_2 bioceramics has progressed, with many reports on their fabrication and characterization of their material properties.[4,5] However, for widespread application of these materials, improvement of biocompatibility is required. One approach to improving the biocompatibility is to infiltrate a bioactive polymer into the porous ceramics. Biopolymer materials have two purposes: to increase the fracture strength by the physical joint and reduce the stiffness of porous ceramics.

The infiltration process has been recognized as one of the most effective methods for production of composite materials.[6,7] It has been used industrially for both polymer and metal matrix composites,[8] and now it has also emerged as one of the most promising pathways to the productions of ceramic matrix composites.[9,10] In the infiltration process, the interconnected pores in the porous materials are replaced with liquid materials. This allows a "continuous" distribution of the polymer throughout the structure, and hence a good transmission of the stress between phases, which results in higher-quality mechanical properties.

To obtain sound porous ceramics, the relationship between the mechanical behavior and the microstructure must be carefully characterized. The porosity and connectivity of open pores, which are the main filtration-parameters, should be controlled. The pore-forming agent determines the homogeneous distribution of pores during the manufacturing process.

Currently, the infiltration of a polymer into porous ceramic bodies is performed via several approaches, including solvent infiltration, melt infiltration, and monomer and initiator infiltration followed by in-situ polymerization.[9, 11] In this work, porous Al_2O_3-(m-ZrO_2) composites were fabricated by pressureless sintering. To obtain Al_2O_3-(m-ZrO_2)/polymer hybrid composites, PMMA was infiltrated into the porous Al_2O_3-(m-ZrO_2) composites. This method employed the sintering process for the preparation of the Al_2O_3-(m-ZrO_2) scaffold, but the subsequent hybridization of the scaffold with PMMA phases was carried out through an infiltration route. This study focused on the characterization of the relationship between the microstructure and the material properties, such as elastic modulus and bending strength, in the porous Al_2O_3-(m-ZrO_2) composites and the Al_2O_3-(m-ZrO_2)/PMMA hybrid composites.

†Corresponding author : Byong-Taek Lee
E-mail : lbt@sch.ac.kr
Tel : +82-41-570-2427 Fax : +82-41-577-2415

2. Experimental Procedure

To fabricate the porous Al_2O_3-ZrO_2 composites, Al_2O_3 (about 300 nm, Sumitomo, Japan), monoclinic Zirconia (m-ZrO_2) (about 70 nm, Tosho, Japan), and PMMA (range of about 200 - 250 μm, LG chemical company, Korea) as a pore-forming agent were used. The first Al_2O_3 and m-ZrO_2 (25 wt %) powders were mixed for 24 h by wet-ball milling using Al_2O_3 balls, and then the mixture powders were dried on a hot plate while stirring. The Al_2O_3-(m-ZrO_2) powders and different volume percentages (40, 45, 50, 55, 60 vol %) of PMMA powders were mixed for 15 h by dry-ball milling also using Al_2O_3 balls. The mixture powders were compacted into pellets by a uniaxial press. The green pellets were burned out in air atmosphere at 1000°C, and the heating rate was 30°C/h for easy evaporation of the volatile components as well as for prevention of bulk defects, such as cracks and swelling. The post-burn-out samples were sintered at 1400°C and 1500°C for 1 h in air atmosphere. In addition, PMMA dissolved in ethanol solvent was poured into a mold which contained porous Al_2O_3-(m-ZrO_2) composites. After complete solidification of the PMMA solution, the PMMA on the outside of the samples was removed to yield Al_2O_3-(m-ZrO_2)/PMMA composites.

Analyses of the PMMA weight loss dependent on the increase of temperature were carried out via thermo-gravimetric analysis (TG, SDT Q600, TA instruments) and differential thermal analysis (DTA, SDT Q600, TA instruments). The relative densities of the porous Al_2O_3-(m-ZrO_2) bodies before and after infiltration of PMMA were measured by the Archimedes method. The pore size and microstructure of the porous Al_2O_3-(m-ZrO_2) composites before and after infiltration were investigated by scanning electron microscopy (SEM, JSM-635F, Jeol). The hardness was measured using a Vickers hardness tester (Hv-112, Akashi, Japan) by indenting with a load of 0.5 kg (10 points/sample). To assess the bending strength and elastic modulus measurements, bar-shaped samples were fabricated ($4 \times 4.5 \times 35$ mm^3). The bending strength measurement was carried out via a four-points bending method with a span length of 10 mm and a crosshead speed of 0.1 mm/min, using a universal testing machine (Unitech^{TM}, R&B, Korea). The elastic modulus was calculated using the following equation, which was developed by Grindosonic (J. W. Lemmens, MK5).[12]

$$E_R = 0.9465 \times \frac{M \times f^2}{w} \times \frac{L_T^3}{t^3} \times \left[1 + 6.59 \times \left(\frac{t^2}{L_T^2}\right)\right]$$

where E_R is the elastic modulus, M is the weight, f is the frequency, w is the width, L_T is the length, and t is thickness of

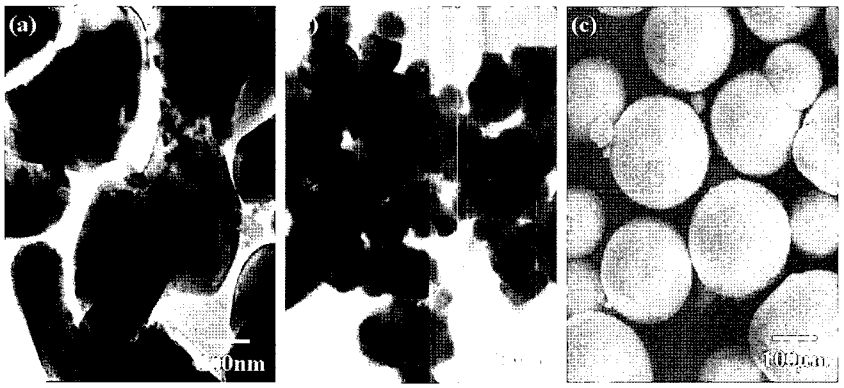

Fig. 1. TEM micrographs of (a) raw Al_2O_3, (b) m-ZrO_2 powder, and (c) SEM micrograph of PMMA powder.

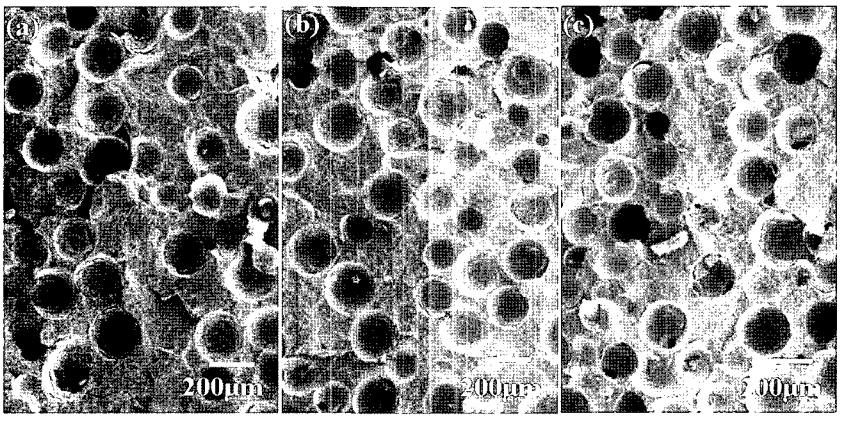

Fig. 2. SEM micrographs of porous Al_2O_3-(m-ZrO_2) composites, depending on the PMMA content: (a) 40 vol %, (b) 50 vol %, and (c) 60 vol %.

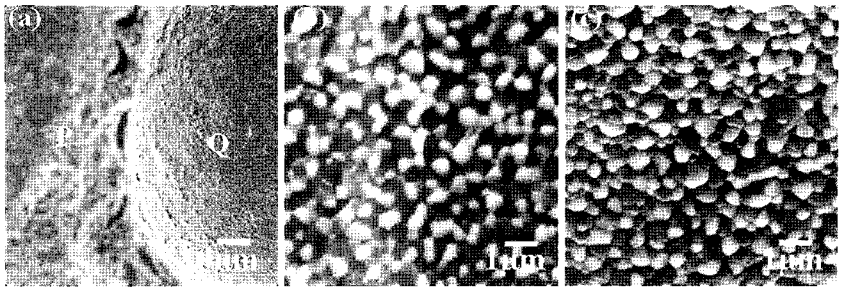

Fig. 3. SEM micrographs of porous Al_2O_3-(m-ZrO_2) composites (a) after thermal etching at 1300°C, (b) enlargement of P region, and (c) enlargement of Q region.

a specimen. When the elastic modulus was calculated, average values (more than 10 times) were used.

3. Results and Discussion

Fig. 1 shows TEM micrographs of (a) raw Al_2O_3 powder, (b) m-ZrO_2 powder, and (c) an SEM micrograph of raw PMMA powder that was used as a pore-forming agent. The average particle sizes of the raw Al_2O_3 and ZrO_2 powders were about 300 nm and 70 nm, respectively, and the PMMA powder was spherical-shaped and about 200-250μm in diameter.

Fig. 2 shows SEM micrographs of porous Al_2O_3-(m-ZrO_2) composites, depending on the PMMA content. After the second burn-out and sintering process, the pore-forming agent (PMMA) was clearly removed and no bulk defects, such as shrinkage or cracks, were found in the porous bodies. Spherical-shaped pores about 200 μm in diameter were homogeneously dispersed in the Al_2O_3-(m-ZrO_2) matrix. This observation revealed that the pore size in the porous bodies slightly decreased compared with that of raw PMMA powders, which was due to the densification of porous Al_2O_3-(m-ZrO_2) bodies during the sintering process. As the PMMA content increased, the number of pores significantly increased. However, in the case of 60 vol % PMMA content, many pores were connected with surrounding pores. The connectivity is the most important factor in making the infiltration of the polymer easy.

Fig. 3 shows SEM micrographs of porous Al_2O_3-(m-ZrO_2) composites after thermal etching at 1300°C. The enlarged images of (b) and (c) were taken from the pore frame (marked P) and the inner region of a pore (marked Q). In these images, the many grains with bright contrast correspond to the ZrO_2 particles and are homogeneously dispersed in the Al_2O_3 matrix. However, the enlarged (b) and (c) micrographs show slightly different images, i.e., the grain morphology in (c) the pore region was rougher than that of (b) the pore frame. This is may be due to the different condition of the sample before the thermal etching, i.e., the pore frame region was clearly polished, but the pore region was not well polished due to its curved shape.

Fig. 4 shows an SEM micrograph and TG/DTA profiles of PMMA powder for the infiltration. The average particle size of the PMMA powder ranged from 20 to 25 μm in diameter, though some particles were less than 10 μm in diameter. In this work, fine-sized PMMA powder particles were used because they can be easily dissolved using an acetone agent. TG and DTA profiles of the PMMA powder are shown in

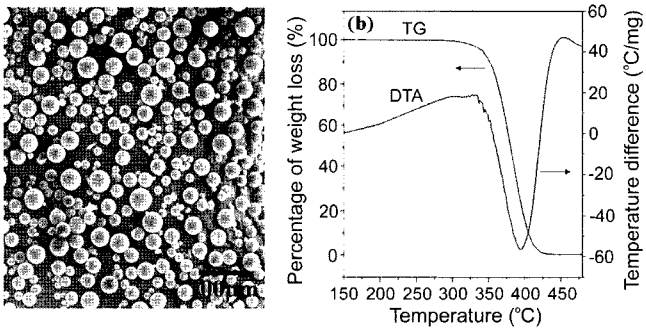

Fig. 4. SEM micrographs and TG/ DTA profiles of PMMA powders.

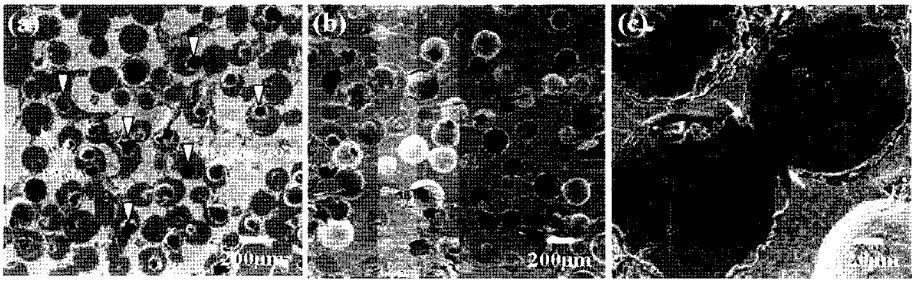

Fig. 5. SEM micrographs of Al_2O_3-(m-ZrO_2)/PMMA hybrid composites: (a) plane view, (b) cross sectional view, and (c) enlarged image.

Fig. 4(b). In the TG profile, the percentage of weight of PMMA powder decreased as the temperature increased to 340°C. However, at over 425°C, the PMMA powder was completely removed. On the other hand, in the DTA profile, an endothermic reaction occurred at around 380°C due to the decomposition of the PMMA powder.

Fig. 5 shows SEM micrographs of Al_2O_3-(m-ZrO_2)/PMMA hybrid composites made by the infiltration of the PMMA solution. In this case, the porous Al_2O_3-(m-ZrO_2) composites using 60 vol % PMMA content were used. In Fig. 5(a), the plane view observation, most of the pore regions were infiltrated with the PMMA phase, but a few pores, as indicated with arrowheads, were not fully infiltrated. However, in Fig. 5(b), the cross-sectional observation, many residual pores were observed without infiltration in the central region of the samples, as indicated with arrowheads, which is basically due to the poor connectivity of open pores. In this image, the edges of the top and bottom sides correspond to the surface regions of the sintered body. However, some regions were fully infiltrated with PMMA due to the necking regions of open pores, as marked with arrows in Fig. 5(c). This observation shows that the PMMA content should be increased to form interconnected pores in the sintered body.

Fig. 6 shows the relative density and bending strength of porous Al_2O_3-(m-ZrO_2) composites and Al_2O_3-(m-ZrO_2)/polymer hybrid composites, depending on the PMMA content that was used as the pore-forming agent. The values of relative density of porous Al_2O_3-(m-ZrO_2) composites significantly decreased as the PMMA content increased. Thus, in the porous Al_2O_3-(m-ZrO_2) bodies sintered at 1400°C and 1500°C using 60 vol % PMMA content, the relative density values were about 42.3% and 45.1%, respectively. However, after PMMA infiltration, the relative densities of the Al_2O_3-(m-ZrO_2)/PMMA hybrid composites were not remarkably increased as the PMMA content used as pore-forming agent increased. In the Al_2O_3-(m-ZrO_2)/PMMA hybrid composites, which were made using 60 vol % PMMA content, the relative density was about 57.3%. These results indicated that PMMA was not fully infiltrated into the central region of porous Al_2O_3-(m-ZrO_2) bodies, as seen in Fig. 5(b). On the other hand, the bending strength values of porous Al_2O_3-(m-ZrO_2) bodies ranged from about 3.5 to 7.2 MPa, which is significantly low compared with that of human bone.[13-15] However, after infiltration, the bending strength of Al_2O_3-(m-ZrO_2)/PMMA hybrid composites increased remarkably as the PMMA content increased. Thus, when using 60 vol % PMMA content to make porous bodies, the value of bending strength of Al_2O_3-(m-ZrO_2)/PMMA hybrid composites was about 33.3 MPa.

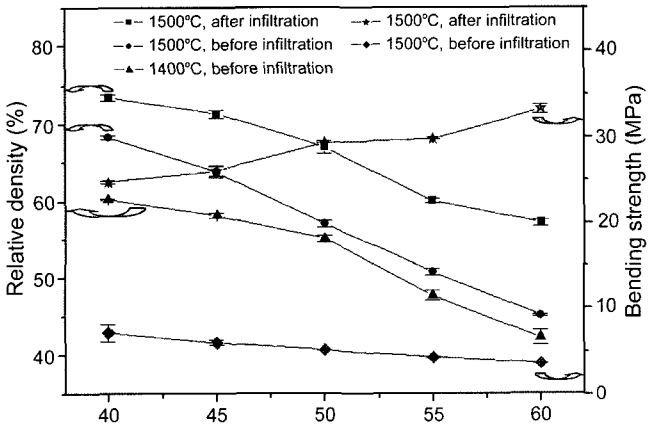

Fig. 6. Relative density and bending strength of porous Al_2O_3-(m-ZrO_2) composites, depending on the PMMA content.

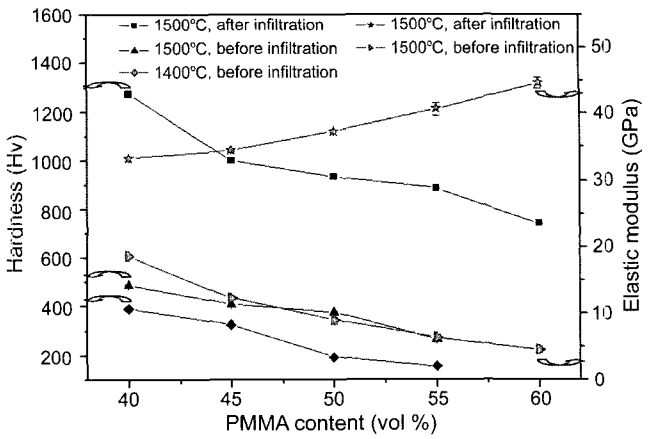

Fig. 7. Hardness and elastic modulus of porous Al_2O_3-(m-ZrO_2) composites, depending on the PMMA content.

Fig. 7 shows the hardness and elastic modulus of porous Al_2O_3-(m-ZrO_2) composites and Al_2O_3-(m-ZrO_2)/PMMA hybrid composites, depending on the PMMA content that was used as a pore-forming agent. The values of the hardness and elastic modulus of the porous bodies slightly decreased as the PMMA content increased. Thus, the hardnesses of the porous Al_2O_3-(m-ZrO_2) bodies sintered at 1400°C and 1500°C, using 55 vol % PMMA, were about 154.9 Hv and 266.4 Hv, respectively. However, the hardnesses of the porous bodies using 60 vol % PMMA couldn't be measured due to their weak bulk bodies. After infiltration of PMMA, the hardness values measured on the surface regions of the infiltrated bulk bodies remarkably increased. On the other hand, the elastic modulus values of the Al_2O_3-(m-ZrO_2)/PMMA hybrid composites increased as the PMMA content used as pore-forming agent increased. Thus, in the sample made using 60 vol % PMMA content, the values for hardness and elastic modulus were about 740.4 Hv and 44.7 GPa, respectively. This result showed that the elastic modulus of the Al_2O_3-(m-ZrO_2)/PMMA hybrid composites was almost the same as human cortical bone.[13-15]

Fig. 8 shows the SEM fracture surfaces of porous Al_2O_3-(m-ZrO_2) and Al_2O_3-(m-ZrO_2)/PMMA hybrid composites. In Fig. 8(a), a low magnification image, it was confirmed that many spherical-shaped pores were homogeneously dispersed on the fracture surface, which was rough. In Fig. 8(b), an enlarged image of the Al_2O_3-(m-ZrO_2) matrix, many

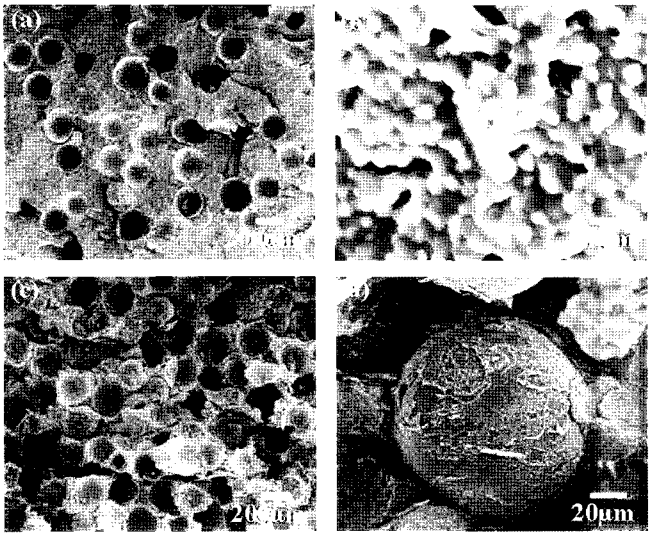

Fig. 8. SEM micrographs showing the fracture surfaces of porous Al_2O_3-(m-ZrO_2) composites: (a) before infiltration, (b) enlarged image of pores frame region, (c) after infiltration, and (d) enlargement of pore after infiltration.

fine pores of about less than 1 μm in diameter were found, and the main fracture mode was a transgranular type, although a few intergranular types with rough surface were also observed. In the Al_2O_3-(m-ZrO_2)/PMMA hybrid composites, the fracture surface near the PMMA regions was remarkably different from that of the porous Al_2O_3-(m-ZrO_2) composite; i.e., many microcracks were found in the Al_2O_3-(m-ZrO_2) pore frame as well as in the pore regions. Furthermore, the fracture surface had a rough morphology due to the existence of the PMMA spheres and their traces. Fig. 8(d) shows one example of a pulled-out PMMA sphere on the fracture surface. The surface morphology of the pulled-out PMMA region was compared with that of raw PMMA powders (Fig. 1 (c)).

In general, for the application of bioceramics as an artificial bone substitute, the mechanical properties, such as fracture strength and elastic modulus, as well as biocompatibility, should have similar values to those of human bone. However, in dense Al_2O_3, ZrO_2, and/or their composite bodies, the elastic modulus values are much higher than that of natural bone (about 10 times). When ceramics with a high elastic modulus have been implanted into a human body, severe bone damage has occurred due to stress shielding and stress concentration effects. There have been many studies on decreasing the elastic modulus of bioceramics[16-18] through the introduction of high porosity. In this maner, the fracture strength is significantly decreased as the elastic modulus is decreased. When a bone substitute is attached to human bone by surgical operation, the artificial bone must be reasonably strong. In the present work, reasonable values of fracture strength and elastic modulus were obtained by the fabrication of Al_2O_3-(m-ZrO_2)/PMMA hybrid composites using the PMMA infiltration method. For the full infiltration of various kinds of biopolymers, pore connectivity should be controlled by homogeneous dispersion and by the addition of an optimal amount of a pore-forming agent.

4. Conclusion

Porous Al_2O_3-(m-ZrO_2) composites were fabricated by pressureless sintering using different percentages (40-60%) of PMMA powders as a pore-forming agent. The pore-forming agent was successfully removed; the pore size and shape were well controlled during the burn-out and sintering processes. The average pore size was about 200 μm in diameter. The material properties of the porous Al_2O_3-(m-ZrO_2) bodies, such as relative density, bending strength, hardness, and elastic modulus were decreased as the PMMA content was increased. Porous Al_2O_3-(m-ZrO_2) composites were infiltrated by the PMMA solution. Most pores on the surface regions of the porous Al_2O_3-(m-ZrO_2) bodies were infiltrated with PMMA, whereas in the central region, many pores without infiltration of PMMA were observed. The bending strength and elastic modulus values of the Al_2O_3-(m-ZrO_2)/PMMA hybrid composites increased to about 33.3 MPa and 44.7 GPa, respectively, which are nearly equivalent to those of human cortical bone.

Acknowledgement

This work was supported by the National Research Laboratory (NRL) research program of the Korean Ministry of Science and Technology.

REFERENCES

1. W. Li and L. Gao, "Fabrication of HAp-ZrO_2 (3Y) Nanocomposite by SPS," *Biomaterials*, **24** 937-3 (2003).
2. G. Willmann, H. J. Fruh and H. G. Pfaff, "Wear Characteristics of Sliding Pars of ZrO_2 (Y-TZP) for Hip Endoprostheses," *Biomaterials*, **17** 2157-5 (1996).
3. W.H. Tuan, R.Z. Chen, T.C. Wang, C.H. Cheng and P.S. Kuo, "Mechanical Properties of Al_2O_3/ZrO_2 Composites," *J. Eur. Ceram. Soc.*, **22** 2827-33 (2002).
4. A. K. Gain, B. T. Lee and H. Y. Song, "Microstructure and Mechanical Properties of Porous Ytria Stabilized Zirconia Ceramic using Poly Methyl Methacrylate Powder," *Scrip. Mater.*, **54** 2081-84 (2006).
5. B. T. Lee, I. C. Kang, A. K. Gain, K. H. Kim and H. Y. Song, "Fabrication of Pore-gradient Al_2O_3-ZrO_2 Sintered Bodies by Fibrous Monolithic Process," *J. Eur. Ceram. Soc.*, **26** 3525-26 (2006).
6. V. Michaud and A. Mortensen, "Infiltration Processing of Fiber Reinforced Composites: Governing Phenomena," *Composites:* Part **A 32** 981-15 (2001).

7. K. Konopka, A. Boczkowska, K. Batorski, M. Szafran and K. J. Kurzydlowski, "Microstructure and Properties of Novel Ceramic-polymer Composites," *Mater. Let.*, **58** 3857-5 (2004).
8. J. A. Cornie, et al, "Processing of Metal and Ceramic Matrix Composites," *Bull Amer. Ceram. Soc.*, **65** [2] 293-11 (1986).
9. W. B. Hillig, "Melt Infiltration Approach to Ceramic Matrix Composites," *J. Amer. Ceram. Soc.*, **71** [2] 96-9 (1988).
10. B. R. Marple, and D. J. Green, "Mullite Alumina Particulate Composites by Infiltration Processing: II, Infiltration and Characterization," *J. Amer. Ceram. Soc.*, **73** [12] 3611-6 (1990).
11. A. A. Abdala, D. L. Milius, D. H. Adamson, I. A. Aksay and R. K. Prud'homme, "Inspired by Abalone Shell: Strengthening of Porous Ceramics with Polymers," *Polyme. Mater: Sci and Engi.*, **90** 384-1 (2004).
12. J. Sabbagh, J. Vreven and G. Leloup, "Dynamic and Static Moduli of Elasticity of Resin-based Materials," *Dental Materials*, **18** 64-7 (2002).
13. K. Rezwan, Q. Z. Chen, J. J. Blaker and A. R. Boccaccini, "Biodegradable and Bioactive Porous Polymer/inorganic Composites Scaffolds for Bone Tissue Engineering," *Biomaterials*, **27** 3413-18 (2006).
14. T. M. Keaveny and W. C. Hayes, "Mechanical Properties of Cortical and Trabecular Bone," *In: Hall BK, p. 285-59, editor. Bone growth. Boca Raton, FL: CRC Press*, 1993.
15. P. Zioupos and J. D. Currey, "Changes in the Stiffness, Strength and Toughness of Human Cortical Bone with Age," *Bone*, **22** 57-9 (1998).
16. A. Wanner, "Elastic Modulus Measurements of Extremely Porous Ceramic Materials by Ultrasonic Phase Spectroscopy," *Mater. Sci. Engi.*, **A 248** 35-8 (1998).
17. W. Pabst, E. Gregorova and G. Ticha, "Elasticity of Porous Ceramics-a Critical Study of Modulus-porosity Relations," *J. Eur. Ceram. Soc.*, **26** 1085-12 (2006).
18. X. D. Ma, T. Ohtsuka, S. Hayashi and Z. Nakagawa, "The Effect of BN Addition on Thermal Shock Behavior of Fiber Reinforced Porous Ceramic Composite," *Comp. Sci. Tech.*, **66** 3089-85 (2006).